Spring Technical Meeting
of the Central States Section of the Combustion Institute
April 22–24, 2012

# A computational investigation of diesel and biodiesel combustion and NOx formation in a light-duty compression ignition engine

*Zihan Wang[1], Kalyan K. Srinivasan[1], Sundar R. Krishnan[1,*], and Sibendu Som[2]*

*[1]Department of Mechanical Engineering, Mississippi State University, MS 39762.*

*[2]Center for Transportation Research, Argonne National Laboratory, Argonne, IL 60439.*

Diesel and biodiesel combustion in a multi-cylinder light duty diesel engine were simulated during a closed cycle (from IVC to EVO), using a commercial computational fluid dynamics (CFD) code, CONVERGE, coupled with detailed chemical kinetics. The computational domain was constructed based on engine geometry and compression ratio measurements. A skeletal n-heptane-based diesel mechanism developed by researchers at Chalmers University of Technology and a reduced biodiesel mechanism derived and validated by Luo and co-workers were applied to model the combustion chemistry. The biodiesel mechanism contains 89 species and 364 reactions and uses methyl decanoate, methyl-9-decenoate, and n-heptane as the surrogate fuel mixture. The Kelvin-Helmholtz and Rayleigh-Taylor (KH-RT) spray breakup model for diesel and biodiesel was calibrated to account for the differences in physical properties of the fuels which result in variations in atomization and spray development characteristics. The simulations were able to capture the experimentally observed pressure and apparent heat release rate trends for both the fuels over a range of engine loads (BMEPs from 2.5 to 10 bar) and fuel injection timings (from 0° BTDC to 10° BTDC), thus validating the overall modeling approach as well as the chemical kinetic models of diesel and biodiesel surrogates. Moreover, quantitative NOx predictions for diesel combustion and qualitative NOx predictions for biodiesel combustion were obtained with the CFD simulations and the in-cylinder temperature trends were correlated to the NOx trends.

## 1. Introduction

With increasing worldwide concern over atmospheric pollution and the shortage of fossil fuels, researchers have been looking for alternative fuels that may provide some solutions. Biodiesel, increasingly accepted as a diesel fuel supplement, is now under extensive research. Biodiesel consists of mono-alkyl esters of long-chain fatty acids from vegetable oils and animal fats [1]. Methanol is usually used in the trans-esterification reaction in biodiesel production, leading to the formation of fatty acid methyl esters [2]. Generally, the common methyl esters found in biodiesel are methyl palmitate ($C_{17}H_{34}O_2$), methyl stearate ($C_{19}H_{38}O_2$), methyl oleate ($C_{19}H_{36}O_2$), methyl linoleate ($C_{19}H_{34}O_2$) and methyl linolenate ($C_{19}H_{32}O_2$). All of them have a methyl ester group attached to a large hydrocarbon chain. Fig. 1 shows the structure of each of these methyl esters.

Compared to conventional diesel, biodiesel fueling of diesel engines produces lower carbon monoxide (CO), unburned hydrocarbon (HC) and particulate matter (PM) emissions [3, 4]. Biodiesel can also be used in current diesel engines with little hardware modifications [5] and is generally compatible with the existing fuel distribution infrastructure in the United States [6].

*Corresponding author: krishnan@me.msstate.edu

However, biodiesel also presents some issues, such as higher oxides of nitrogen (NOx) emissions [3, 4] and decreased oxidative stability [6], that need to be alleviated before wider application can be adopted.

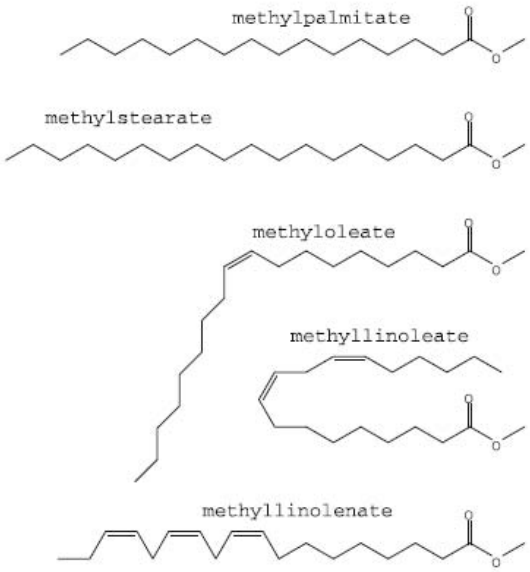


**Figure 1: Five common methyl esters in biodiesel [2]**

The atomization and vaporization behavior of biodiesel and diesel were investigated by Higgins et al. [7], who measured the liquid penetration length of the two fuels in a constant volume combustion vessel at various in-cylinder temperatures and densities. Liquid penetration length is defined as the axial position that encompasses 97 percent of the injected fuel mass at a given time after start of injection (SOI). They found that biodiesel has a higher liquid length at the same condition, due to its higher distillation temperatures. In recent studies by Som et al. [8, 9], the injection and spray characteristics of diesel and biodiesel (from soy-based feedstock) were compared by using an integrated modeling approach. The simulation identified differences in spray characteristics between diesel and biodiesel due to variations in nozzle flow characteristics. Specifically, it was observed that the spray penetration was higher for biodiesel, while the cone angle was smaller. This result was attributed to reduced in-nozzle cavitation and turbulence, which resulted in slower spray breakup for biodiesel and led to increased fuel penetration. To study the combustion behavior of the two fuels, Wu et al. [10] measured the flame lift-off length, which is defined as the farthest upstream location that the diffusion flame can reach. They found that biodiesel has a slightly shorter lift-off length because of its higher flame reactivity.

To understand the potential reasons for NOx increase with biodiesel fueling, Mueller et al. [5] examined and summarized several hypotheses based on the thermal NOx mechanism using experimental data from the Sandia Compression ignition Optical Research Engine (SCORE). It was observed that the higher local oxygen availability and the higher cetane number for biodiesel are responsible for increased NOx emissions, while reduced soot formation and higher adiabatic flame temperatures in biodiesel combustion can only partially explain this problem. They concluded that a combination of several factors could lead to the increased NOx emissions associated with biodiesel combustion, and besides the thermal NO mechanism, engine calibration might also play a role.

Computational fluid dynamics (CFD) provides researchers with supplementary information on key NOx-related species and parameters with spatial and temporal resolution that is not available in current optical research engines. This provides the primary motivation for the present work, i.e., to model biodiesel combustion with a high fidelity and to eventually provide insights regarding the experimentally observed NOx differences between diesel and biodiesel. Therefore, in this paper, the combustion processes of diesel and biodiesel in a four-cylinder light-duty diesel engine were simulated using a multidimensional CFD software (CONVERGE) and compared to experimental results obtained over a range of engine brake mean effective pressures (BMEPs) and fuel injection timings at a constant engine speed of 1800 rev/min.

The CONVERGE CFD software requires chemical reaction mechanisms that can best capture the combustion characteristics of diesel and biodiesel (such as ignition delay and important species history) and are computationally practical. In this study, a skeletal n-heptane-based mechanism developed by researchers at Chalmers University of Technology [11] was used to model diesel combustion chemistry. Recently, researchers at the Lawrence Livermore National Laboratory (LLNL) developed a detailed biodiesel mechanism, containing methyl decanoate (MD, $C_{11}H_{22}O_2$), methyl-9-decenoate (MD9D, $C_{11}H_{20}O_2$), and n-heptane as blend surrogates [12]. Since the LLNL mechanism contains 3299 species and 10806 reactions, it is computationally prohibitive. Therefore, Luo et. al [13] reduced the detailed mechanism with direct relation graph (DRG), isomer lumping, and DRG-aided sensitivity analysis (DRGASA). The validated skeletal mechanism contains 89 reaction and 364 reactions, and is applied in this study to model biodiesel combustion chemistry.

## 2. Formulation of Submodels

### 2.1 NOx Model

Several NOx mechanisms have been adopted in previous engine simulations [14, 15, 16]. The thermal NO mechanism (also known as the extended Zel'dovich mechanism) [17] dominates at high-temperatures over a wide range of equivalence ratios. It is highly sensitive to O, N, and OH species concentrations and their residence time in the high temperature environment. The thermal NO mechanism is relatively well understood. Fenimore [18] proposed the prompt mechanism for NO formation, where some NO is produced in the flame zone of laminar premixed flames (for example), through reactions initiated by methylidyne (CH). The nitrous oxide ($N_2O$) mechanism was also proposed by Wolfrum [19], which considered NO produced by $N_2O$-related reactions. In this study, the NOx formation is modeled using only the thermal NO mechanism that contains the following reactions:

$$O + N2 = NO + N, \quad (1.a)$$

$$N + O2 = NO + O, \quad (1.b)$$

$$N + OH = NO + H. \quad (1.c)$$

If N-atoms are assumed to be in steady state, the production rate of NO can be written as:

$$\frac{d[NO]}{dt} = 2k[O][N_2], \quad (2)$$

where, [ ] designates the mole fraction of each species and $k$ is the reaction rate coefficient. The formation of NOx is generally neglected at temperatures below 1800 K, and as the engine NOx data is reported according to the EPA $NO_2$ based reporting standard, a factor of 1.533 (ratio of $NO_2$ to NO molecular masses) was used to convert the predicted NO to NOx.

2.2 Other Submodels

In addition to the NOx submodel, other dedicated submodels are used to solve each sub-process, including fuel-air interactions, turbulence, combustion, etc. These submodels are listed in Table 1. Among them, the spray breakup model was especially calibrated for fuel-air mixing to ensure reasonable ignition delay and heat release rate predictions. The spray breakup time constant $B_1$ was kept as 28 throughout this study.

**Table 1: The computational submodels applied in this study**

| Phenomenon | Model |
|---|---|
| Spray breakup | KH-RT model [20,21,22] |
| Drop drag | Dynamic model [23] |
| Collision and coalescence | NTC model [24] |
| Drop-wall interaction | Rebound/slide model [25] |
| Vaporization | Multi component fuel |
| Turbulence | RNG $k-\varepsilon$ model [26] |
| Combustion | SAGE [22] |
| Soot Formation | Hiroyasu [27] |

## 3. Results and Discussion

Closed cycle simulations were performed for both diesel and biodiesel combustion using a 3D multiphase CFD tool, CONVERGE [22, 28]. This code applies a novel boundary approach that cuts the intersected cells (cut-cell) at runtime with the user supplied combustion chamber surface data [22]. This technique increases the grid generation and computational efficiency and makes local grid refinement (fixed embedding and adaptive mesh refinement) possible. For all cases, the base grid size is fixed at 1.4 mm in each of the three dimensions. To resolve the flow near the injector, a fixed grid embedding scheme was employed such that the minimum grid size is 0.35 mm. Apart from this region, it is rather difficult to determine *a priori* where grid refinement is needed. Hence, two levels of adaptive mesh refinement were employed for the velocity and temperature fields. As can be seen in Fig. 3, grids around the spray periphery are refined after SOI. The simulations were initialized at Intake Valve Closure (IVC) with uniform temperature, pressure, species mass fractions, turbulence levels, and swirl ratio. Table 2 shows the specifications of the engine and its operating conditions. Since the combustion chamber is not axisymmetric, a 360° full mesh was constructed, as shown in Fig. 2.

**Table 2: Engine specifications and operating conditions**

| Engine Parameter | Specification |
|---|---|
| Engine type | VW 1.9L TDI |
| Bore | 79.5 mm |
| Stroke | 95.5 mm |
| Connecting rod length | 144 mm |
| Compression ratio | 17.0:1 |
| IVC | -125° ATDC |
| EVO | 129° ATDC |

| | |
|---|---|
| Nozzle diameter | 0.205 mm |
| Engine speed | 1800 rpm |
| Swirl ratio | 2.0 (assumed) |
| Rate of injection profile | Top-hat (assumed) |
| BMEP | 2.5, 5, 7.5, 10 bar |
| SOI | -10°, -4°, 0° ATDC |

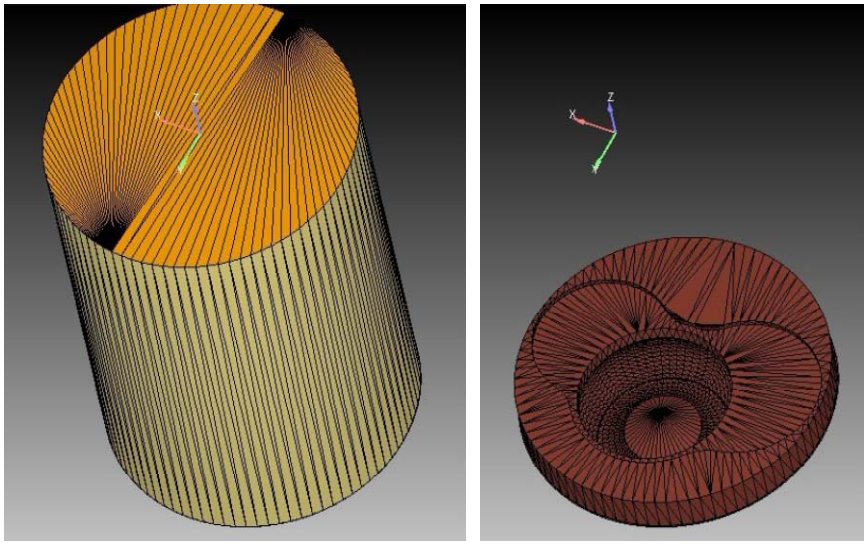

(a) (b)

**Figure 2: (a) The 3D computational domain of the VW engine at BDC and (b) the piston surface grid**

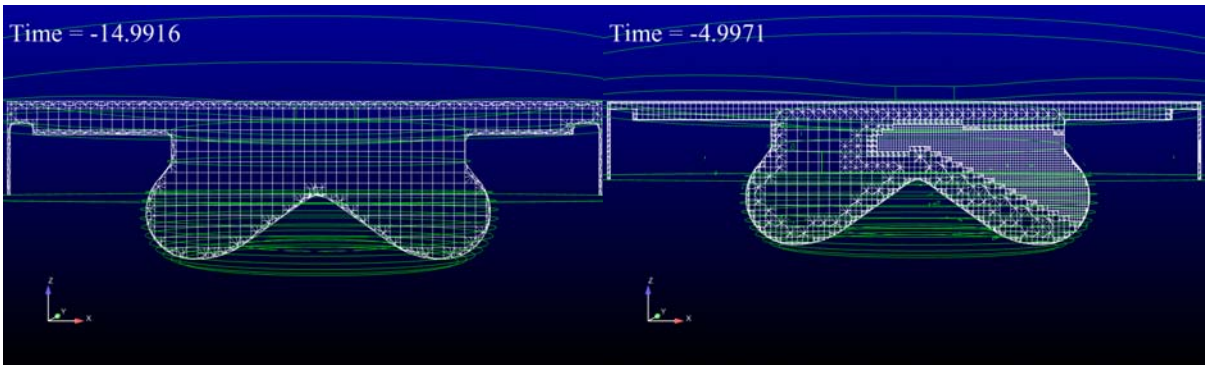


**Figure 3: Grid generated in CONVERGE before (left) and after (right) fuel injection at 10BTDC**

Comparisons of in-cylinder pressure and apparent heat release rates (AHRR) from the diesel combustion simulations and corresponding experiments are shown in Fig. 4. In general, the agreement between experiments and predictions is good. However, the AHRR during the initial ("premixed burn") phase is slightly over-predicted in some cases, especially when injection timings are advanced. This is likely due to uncertainties in the initial conditions (e.g., initial temperatures at IVC), the spray angle, and the rate of fuel injection, which were not measured experimentally. The same comparison is also shown in Fig. 5 for biodiesel combustion at two

different engine loads (BMEP = 5.0 bar and BMEP = 7.5 bar). While the pressures (especially peak pressures) match well by magnitude, the increase in predicted AHRR after ignition is slower compared to the experimental AHRR for all cases with biodiesel, thus affecting the combustion phasing, overall heat release rate, and NOx emissions later in the combustion process. In addition, the peak predicted AHRR values are consistently higher than the corresponding experimental values. Possible reasons for the slower initial AHRR predictions may include uncertainties in initial conditions as well as potential inadequacies related to the low-temperature chemistry in the biodiesel mechanism. The authors are investigating this issue further and hope to address these reasons in future publications.

Figure 6 compares the NOx emissions indices from both diesel and biodiesel combustion at two different engine loads (BMEP = 5 and 7.5 bar). The NOx emissions index is defined as the ratio of the mass of NOx in grams to the mass of fuel injected in kilograms. In this study, NOx emissions are not presented in the commonly used brake specific NOx (BSNOx) format because the simulation does not provide engine brake power. It can be seen that NOx is accurately predicted at all injection timings for diesel combustion, while for the biodiesel cases, the NOx levels were under-predicted by nearly 50 percent. This is very likely linked to the discrepancies between the experiments and simulations in combustion phasing and heat release rates discussed above. Despite the under-prediction of NOx for biodiesel combustion, it must be emphasized that both diesel and biodiesel simulations capture the general NOx trends versus fuel injection timings, i.e., retarded injection timings lead to lower NOx emissions. This trend may be attributed to the retardation in combustion phasing (e.g., CA50) with retarded SOI, thus lowering local temperatures and reducing NOx. One important point to note from Fig. 6 is the fact that, although BSNOx emissions are widely reported to be higher for biodiesel combustion compared to diesel combustion, the NOx emissions per unit mass of fuel consumption is not necessarily higher, as is the case at both loads (observed both experimentally and from the simulations). Since biodiesel has a smaller lower heating value (LHV) compared to diesel, a greater mass of biodiesel is needed to obtain the same load as diesel (assuming the same fuel conversion efficiencies were maintained with both fuels). Therefore, even if the mass of NOx is slightly higher with biodiesel, the NOx emissions expressed as grams per kg of fuel (emissions indices) can still be comparable to diesel combustion values.

According to the thermal NO mechanism, local temperature, local oxygen availability, and residence time (the relative durations for which high-temperature regions persist in the cylinder) can all influence NOx formation. The first factor is analyzed here. Fig. 7 (a) presents the in-cylinder peak temperatures at BMEP = 7.5 bar. Peak temperatures are higher for early injection timings and for diesel combustion. In-cylinder averaged temperatures are shown in Fig. 7 (b) as well to examine the possible offsetting contribution to NOx formation from low temperature cells. Similar trends can be observed in in-cylinder averaged temperatures and peak temperatures. These trends from both temperature traces help to explain the observed (from both experiment and simulation) higher NOx index for advanced SOIs and for diesel combustion in Fig. 5.

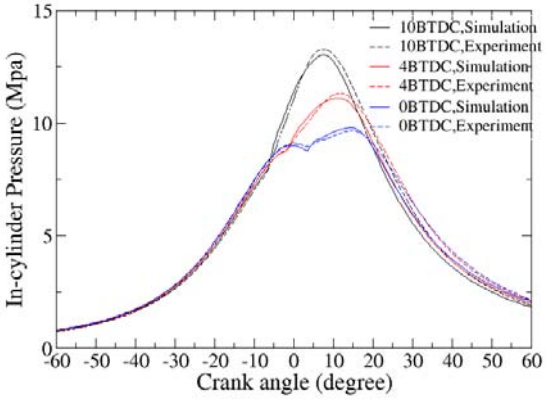
In-cylinder Pressure (Mpa)
Crank angle (degree)
10BTDC,Simulation
10BTDC,Experiment
4BTDC,Simulation
4BTDC,Experiment
0BTDC,Simulation
0BTDC,Experiment

(a)

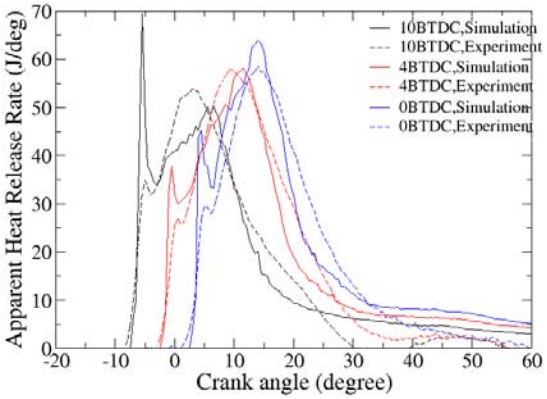
Apparent Heat Release Rate (J/deg)
Crank angle (degree)
10BTDC,Simulation
10BTDC,Experiment
4BTDC,Simulation
4BTDC,Experiment
0BTDC,Simulation
0BTDC,Experiment

(b)

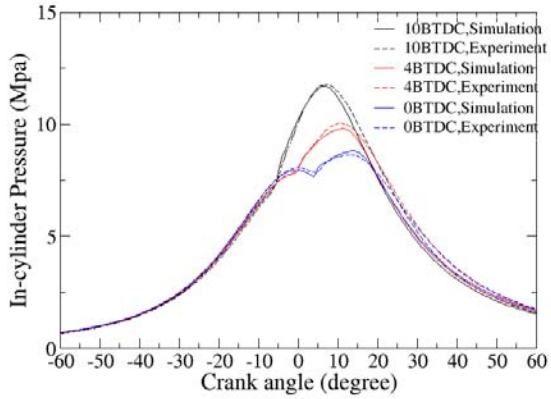
In-cylinder Pressure (Mpa)
Crank angle (degree)
10BTDC,Simulation
10BTDC,Experiment
4BTDC,Simulation
4BTDC,Experiment
0BTDC,Simulation
0BTDC,Experiment

(c)

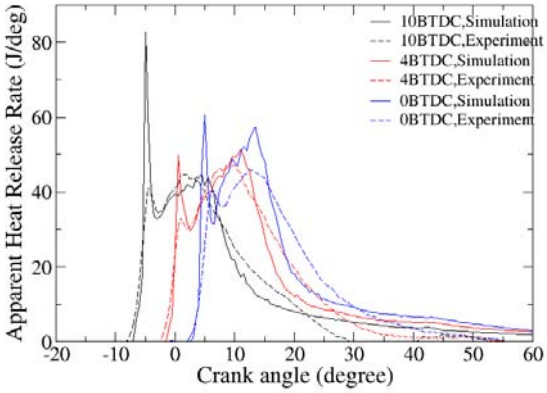
Apparent Heat Release Rate (J/deg)
Crank angle (degree)
10BTDC,Simulation
10BTDC,Experiment
4BTDC,Simulation
4BTDC,Experiment
0BTDC,Simulation
0BTDC,Experiment

(d)

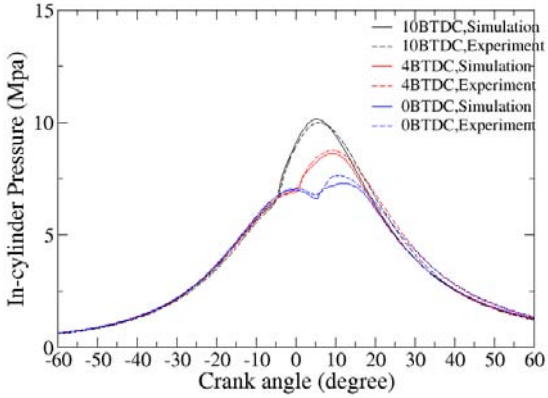
In-cylinder Pressure (Mpa)
Crank angle (degree)
10BTDC,Simulation
10BTDC,Experiment
4BTDC,Simulation
4BTDC,Experiment
0BTDC,Simulation
0BTDC,Experiment

(e)

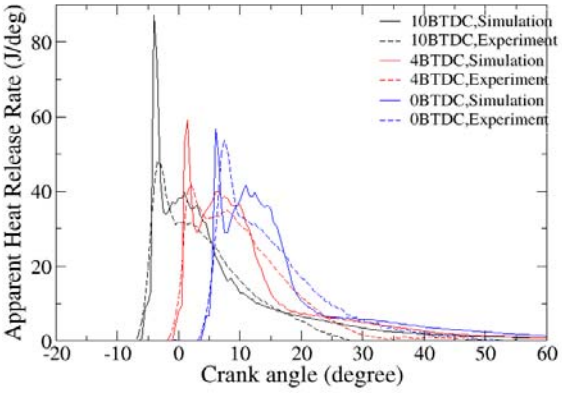
Apparent Heat Release Rate (J/deg)
Crank angle (degree)
10BTDC,Simulation
10BTDC,Experiment
4BTDC,Simulation
4BTDC,Experiment
0BTDC,Simulation
0BTDC,Experiment

(f)

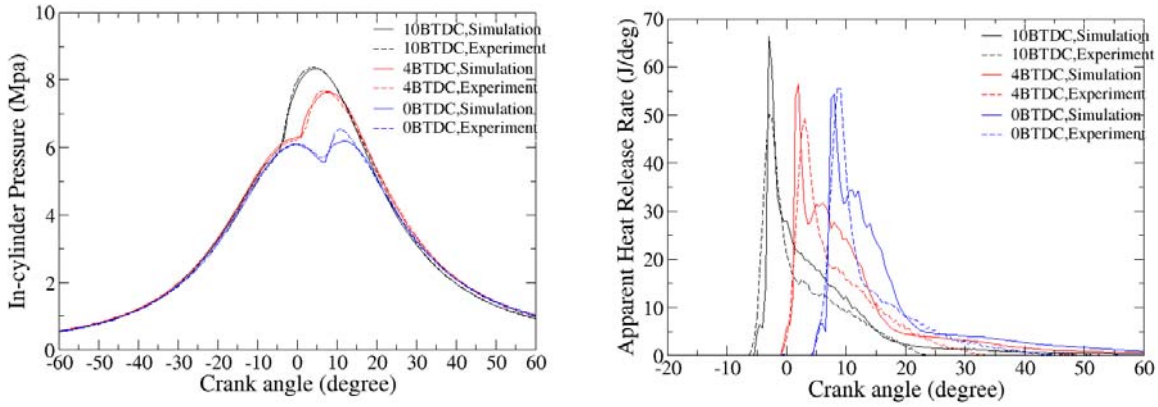


(g) (h)

**Figure 4: Predicted and measured in-cylinder pressure (left) and AHRR (right) for diesel simulations with BMEPs: (from top to bottom) 10, 7.5, 5, and 2.5 bar, and injection timings from 10° BTDC to 0° BTDC**

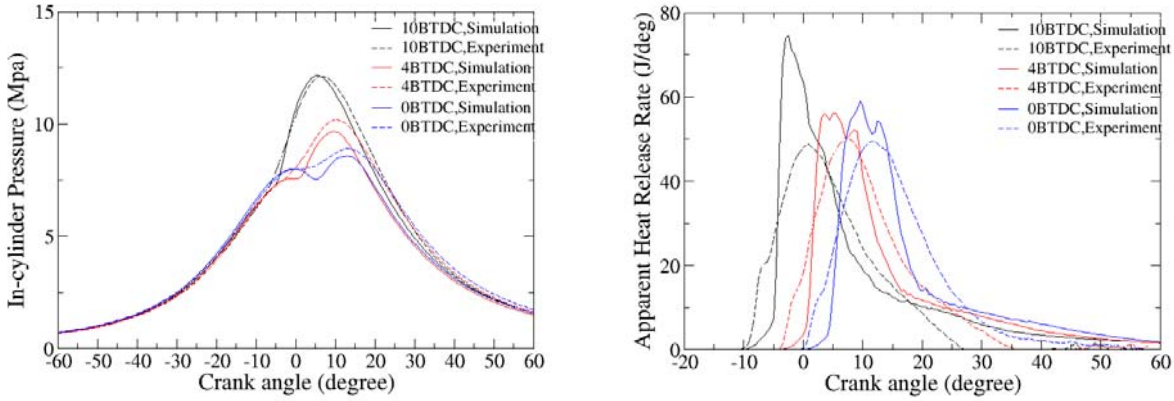


(a) (b)

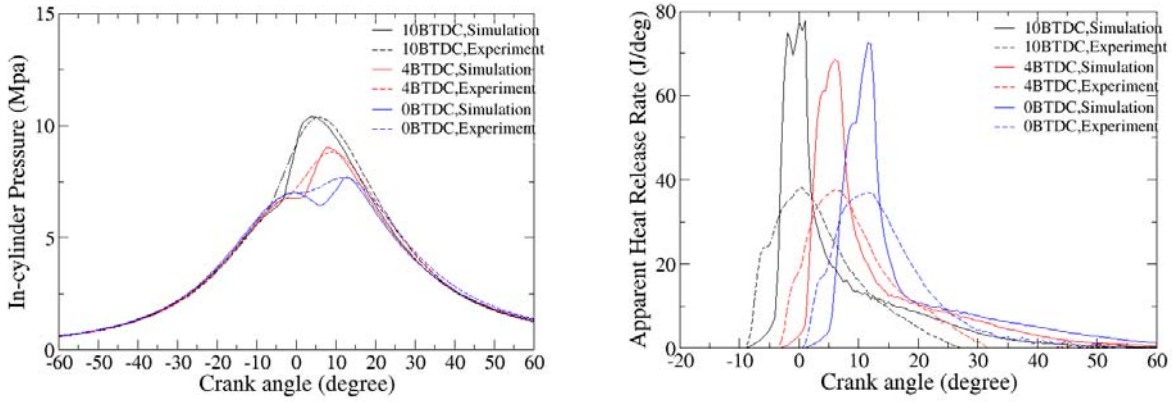


(c) (d)

**Figure 5: Predicted and measured in-cylinder pressure (left) and AHRR (right) for biodiesel simulations with BMEPs: (from top to bottom) 7.5 and 5 bar, and injection timings from 10° BTDC to 0° BTDC**

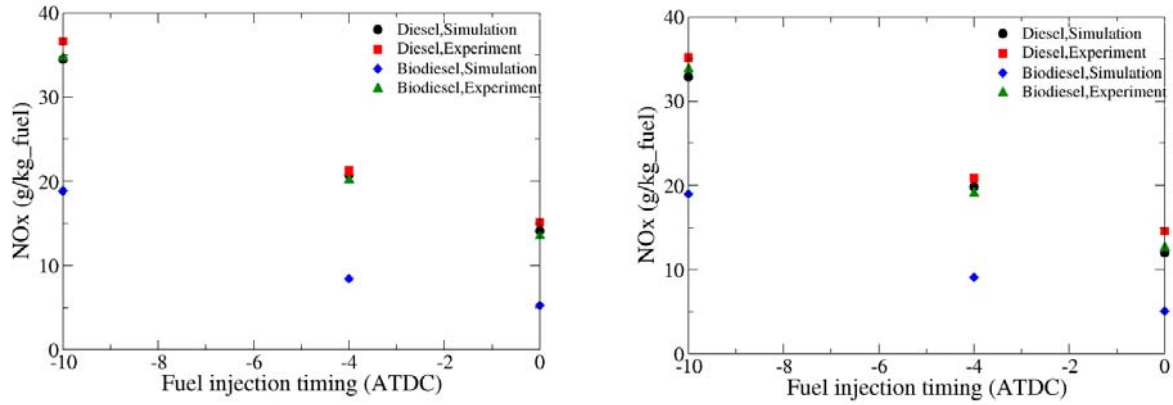


**Figure 6: Measured and predicted NOx emissions versus fuel injection timing for diesel and biodiesel combustion at BMEP = 7.5 bar (left) and 5 bar (right)**

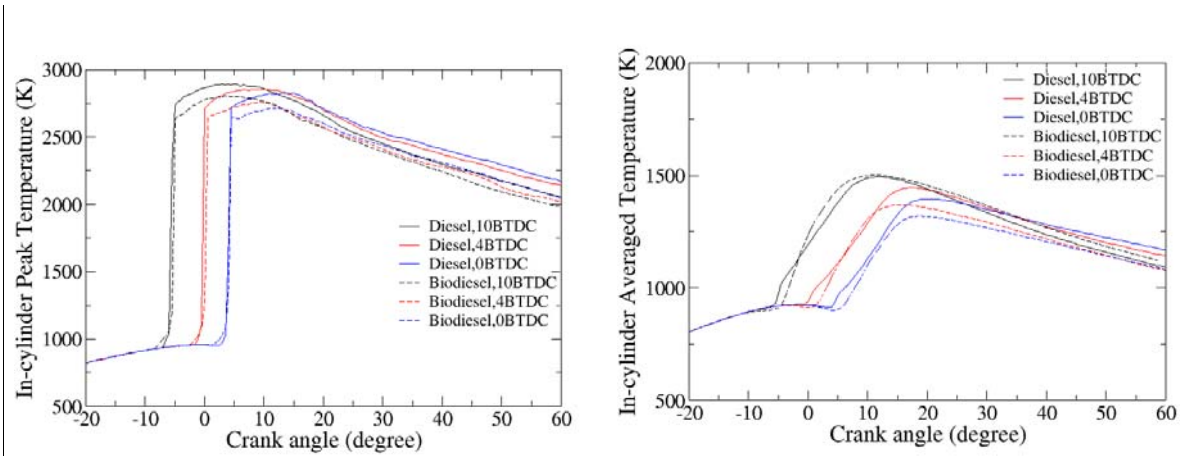


(a) (b)

**Figure 7: In-cylinder peak (a) and averaged (b) temperatures for diesel and biodiesel at BMEP = 7.5 bar**

## 4. Concluding Remarks

In this work, a 3D multiphase CFD software, CONVERGE, was applied to simulate cylinder pressure and heat release histories and NOx emissions for diesel and biodiesel combustion in a light-duty compression ignition engine. The CFD simulation incorporated reduced chemical kinetic mechanisms for diesel and biodiesel surrogates, the thermal NO mechanism, and a suite of submodels related to fuel injection, mixing, and turbulence. With this setup, the current CFD model was able to capture experimentally observed pressure and AHRR trends for diesel combustion, with some discrepancy in biodiesel AHRR predictions. The NOx emissions from diesel combustion were predicted accurately, while they were under-predicted for biodiesel combustion; however, the general trends observed experimentally for NOx emissions versus injection timing were captured well for both diesel and biodiesel combustion. Retarded fuel injection timing can help reduce NOx emissions as a result of retarded combustion phasing (lower temperature). Additional work is necessary to improve the NOx predictions for biodiesel combustion, along with the associated AHRR phasings and magnitudes.

## Acknowledgments

This material is based upon work performed through the Sustainable Energy Research Center at Mississippi State University and is supported by the US Department of Energy under Award Number DE-FG3606GO86025.

The submitted manuscript has been created by UChicago Argonne, LLC, operator of Argonne National Laboratory (Argonne). Argonne, a U.S. Department of Energy Office of Science laboratory, is operated under Contract No. DE-AC02-06CH11357. The U.S. Government retains for itself, and others acting on its behalf, a paid-up, nonexclusive, irrevocable worldwide license in said article to reproduce, prepare derivative works, distribute copies to the public, and perform publicly and display publicly, by or on behalf of the Government.

## References


[1] ASTM International Specification: ASTM D 6751, 2008.
[2] O. Herbinet, W. J. Pitz, C. K. Westbrook, *Combustion and Flame* 154 (2008) 507–528.
[3] M. S. Graboski, R. L. McCormick, *Progress in Energy and Combustion Science* 24 (1998) 125–164.
[4] M. Lapuerta, O. Armas, J. Rodriguez-Fernandez, *Progress in Energy and Combustion Science* 34 (2008) 198–223.
[5] C. J. Mueller, A. L. Boehman, G. C. Martin, *SAE 2009-01-1792* (2009).
[6] G. Knothe, *Energy and Fuels* 22 (2008) 1358–1364.
[7] B. S. Higgins, C. J. Mueller, D. L. Siebers, *SAE 1999-01-0519* (1999).
[8] S. Som, PhD thesis, University of Illinois at Chicago, 2009
[9] S. Som, et. al, *Fuel* 89 (2010) 4014-4024.
[10] Y. Wu et al., *SAE 2010-01-0606* (2010).
[11] http://www.tfd.chalmers.se/ valeri/MECH.html
[12] O. Herbinet, W. J. Pitz, C. K. Westbrook, *Combustion and Flame* 157 (2010) 893–908.
[13] Z. Luo et al, Accepted to *Combustion Theory and Modeling* (2012).
[14] Y. Ren, X. Li, *SAE 2011-01-1385* (2011).
[15] W. L. Cheng, C. F. Lee, D. F. Ruan *SAE 2008-01-1638* (2008).
[16] J. Yang et. at, *SAE 2011-01-1929* (2011).
[17] J. B. Heywood, *Internal Combustion Engine Fundamentals*, McGraw-Hill, Inc.,1988.
[18] C. P. Fenimore, 13$^{th}$ Symp (Int) on Combustion, 13 (1971) 373–380.
[19] J. Wolfrum, *Chemie-Ingenieur-Technik* 44 (1971) 656
[20] R. D. Reitz, *Atomization and Spray Technology*, 3 (1987) 309–337.
[21] T. F. Su et al *SAE 960861* (1996).
[22] K. J. Richards, P. K. Senecal, E. Pomraning, *CONVERGE(Version 1.3)*, Convergent Science, Inc., Middleton,WI, 2008.
[23] A. B. Liu, D. K. Mather, R. D. Reitz, *SAE 930072* (1993).
[24] D. P. Schmidt, C. J. Rutland, *Journal of Computational Physics*, 164 (2000) 62.
[25] J. Naber, R. D. Reitz, *SAE 880107* (1988).
[26] S. C. Kong, Z. Han, R. D. Reitz, *SAE 950278* (1995).
[27] H. Hiroyasu, T. Kadota, *SAE 760129* (1976).
[28] P. K. Senecal et al, *SAE 2007-01-0159* (2007).